Materials Characterization 122 (2016) 170–176

Contents lists available at ScienceDirect

Materials Characterization

journal homepage: www.elsevier.com/locate/matchar

Effect of wheel speed and annealing temperature on microstructure and texture evolution of $Ni_{45}Mn_{36.6}In_{13.4}Co_5$ ribbon

Yan Feng [a,*], Hong Chen [a], Li Gao [b], Haibo Wang [c], Xiaohai Bian [a], Mingjie Gong [a]

[a] State Key Laboratory of Solidification Processing Northwestern Polytechnical University, Xi'an, Shaanxi 710072, PR China
[b] College of Engineering Science and Technology, Shanghai Ocean University, Shanghai 201306, PR China
[c] College of Physics and Electronic Engineering, Taizhou University, Taizhou, Zhejiang 318000, PR China

ARTICLE INFO

Article history:
Received 9 August 2016
Received in revised form 19 October 2016
Accepted 27 October 2016
Available online 29 October 2016

Keywords:
Magnetic shape memory alloy
Melt-spun ribbon
Annealing
Texture
Electron back scatter diffraction (EBSD)

ABSTRACT

$Ni_{45}Mn_{36.6}In_{13.4}Co_5$ magnetic shape memory alloy was successfully produced as preferentially textured ribbon by melting spinning with different wheel speed. X-ray diffraction (XRD) and electron back scatter diffraction (EBSD) were used to study structure and texture evolution of these melt-spun ribbons. The thickness of melt-spun ribbon is 42 μm, 65 μm and 30 μm depending on wheel speed of 1 0 m/s, 15 m/s and 20 m/s, respectively. Density of α fiber texture (⟨100⟩//ND) vary with wheel speed changes, and is most intensive in the ribbon with wheel speed of 15 m/s. Grains of the ribbons grow after being annealed at 873 K, 973 K, 1073 K and 1173 K, recrystallization was not observed in ribbons after being annealed at 873 K but occurred in ribbons after being annealed at higher temperatures. The α fiber texture becomes weaker to some extent after annealing at different temperatures, due to new recrystallization texture formed at the process of annealing.

1. Introduction

Magnetic shape memory alloy has been widely investigated in the past decades due to their large magnetic field induced strain (MFIS) and high frequency response [1–6]. MFIS is obtained mainly through the movement of martensitic twin boundary or phase transformation in magnetic field [7,8]. In 1996, Ullakko et al. firstly reported that NiMnGa alloy shows large strain via the twin variants rearrangement in martensitic state when it was subjected to an applied magnetic field [9]. Until now, magnetic field induced strain of up to 10% has been realized in off-stoichiometric $Ni_{48.8}Mn_{29.7}Ga_{21.5}$ single crystal [10]. But even for NiMnGa single crystal, the magnetocrystalline anisotropy energy (MAE) which is the source of martensite twin reorientation is limited, that leads to low magnetostress of only several megapascals [11]. Phase transformation induced by field is also achieved in NiMnGa under special conditions such as at temperature very close to A_S or when X-phase was observed [12,13]. But the value of magnetostress is still low, because the available magnetic energy which provides phase transformation Zeeman energy is limited under magnetic field. Thus, low magnetostress limits the potential applications of NiMnGa alloys as magnetic actuators. Other NiMn-based magnetic shape memory alloys such as NiMnIn [14], NiMnSn [15], and NiMnSb [16] exhibit reversible phase transformation more easily under magnetic field, due to the giant magnetization difference between austenite and martensite which provides phase transformation Zeeman energy under magnetic field. Therefore, those alloys show high magnetic field induced stress across the austenite-martensite transformation, and it should be noted that the Zeeman energy increases with applying of magnetic field. Karaca et al. observed a high magnetostress of approximately 30 MPa under 1.6 T magnetic field in NiMnInCo alloys which is nearly five times higher than that observed in NiMnGa alloys [17]. The high magnetostress makes the application as magnetic actuation possible. Whereas, in NiMnIn (Sn, Sb) alloys large magnetic field induced strain and high magnetostress were also obtained in single crystal [18]. However, the preparation of single crystal is a time and cost consuming process, and segregation caused by the compositional change along the axis of the crystal is harmful for the performance of the alloy [19]. Polycrystalline sample with coarse-grain and strong texture is similar to a single crystal [20]. The effect of texture on magnetostress and recoverable strains in shape memory alloy have been systematically studied by R.V. Kohn [21], the polycrystal with texture has large magnetocrystalline anisotropy which can increase recoverable strains effectively. The textures in hot rolled NiMnGa shape memory alloy had been investigated by Tomasz Goryczka [22].

Melt spinning technique was widely used to prepare thin NiMn-based magnetic shape memory ribbons with columnar crystals perpendicular to ribbon surface [23,24,25]. This technique offers two potential advantages for the fabrication of magnetic shape memory alloys: the composition is homogeneous, and it is easy to get highly textured polycrystalline ribbons [26]. Electron back scatter diffraction (EBSD) has made an impressive impact on the characterization of materials by directly linking microstructure and crystallographic texture, which provides very rich and quantitative datasets [27]. EBSD has been used

* Corresponding author.
E-mail address: yanfeng@nwpu.edu.cn (Y. Feng).

http://dx.doi.org/10.1016/j.matchar.2016.10.030
1044-5803/

to identify Constraint-dependent twin variant distribution in Ni_2MnGa single crystal, polycrystal and thin film successfully [28]. Thus, the formation and evolution of texture and microstructure in $Ni_{45}Mn_{36.6}In_{13.4}Co_5$ melt-spun ribbons are investigated by using EBSD, and the influence of wheel speed and annealing temperature are discussed in detail.

2. Material and Methods

Ingots with nominal composition of $Ni_{45}Mn_{36.6}In_{13.4}Co_5$ were prepared by arc melting the pure metals under argon atmosphere in a water-cooled Cu crucible, and they were remelted several times to ensure the homogeneity. The ingots were cut into small bulks with wire-electrode cutting, which were induction melted in a quartz tube and ejected with 0.02 MPa pressurized argon onto water cooled copper wheel with rotating linear speed (Vs) of 10 m/s, 15 m/s and 20 m/s, respectively. The ribbons were sealed in quartz tube at vacuum of 10^{-3} Pa and annealed for 1 h at 873 K, 973 K, 1073 K, 1173 K respectively. Differential Scanning Calorimetry (DSC) results showed that the martensitic transformation temperature (M_s) of $Ni_{45}Mn_{36.6}In_{13.4}Co_5$ ribbon was below room temperature, it illustrated that the melt-spun ribbons were in the state of parent phase at room temperature. The preferred orientation and phase structure were studied by X-ray diffraction (XRD; PANALYFICAL X'Pert PRO) by using Cu Kα radiation. The microstructure and texture analysis were carried out by EBSD techniques. We firstly studied the cross section of melt-spun ribbons, which were mounted into electroconductive resin carefully to ensure the perpendicularity. The samples were polished by mechanical and vibrating methods before EBSD experiment. All EBSD experiments were carried out at room temperature by using the Scanning Electron Microscope (TESCAN Mira3) equipped with an EBSD Nordlys detector. EBSD maps were collected with the scanning step size varying from 0.3 to 0.7 μm, depending on the grain size. The grain orientation and the grain reconstruction were analyzed by using HKL CHANNEL5 package software. The pixel color of EBSD maps represented the unit cell orientation. The indexing rate, i.e. the fraction of pixels in EBSD maps, of which the unit cell orientation could be successfully indexed, depended on the surface quality and of sample and how the real structure and structure in database matched. In our experiment results, the indexing rates of all the raw EBSD maps were high (above 90%).

3. Results and Discussion

3.1. Preferred Orientation and Phase Structure Depending on Wheel Speed

The X-ray diffraction patterns of melt-spun ribbons prepared by different wheel speeds are shown in Fig. 1. The X-ray diffraction spectrum indicates that $Ni_{45}Mn_{36.6}In_{13.4}Co_5$ alloy is austenitic phase at room temperature, but in bulk alloys the atomic order is distinctly, austenitic phase is embodied as the difference between the fully ordered $L2_1$ phase and the partially-ordered B2 phase [29]. During the solidification, the melt solidifies into the B2 structure at first, and then reaches $L2_1$ austenite structure through a second-order B2–$L2_1$transition [30–33]. Compared with the water-quenching process in bulk alloys, the melt-spinning technique is expected to generate a higher disorder in the structure of ribbons [34]. XRD patterns in Fig. 1 show that all as-spun ribbons with different wheel speed are partially-ordered B2 phase at room temperature, with strong (200), (220), (400), (422) reflections. The superlattice peak (111) reflection which indicate the ordered structure will appears after certain temperature annealing in later result. The most intensive peak of bulk sample with random orientation appears at the position of $2\theta = 42.6°$, corresponding to the diffraction of (220) plane of B2 parent phase [34]. However, the most intensive of ribbons is corresponding to the diffraction of (400) plane, indicating that the ⟨100⟩ direction of parent phase is the preferred direction during the rapid solidification process. The relative intensity of main diffraction peaks can be employed to analyze the preferential orientation under the same detecting condition. As shown in Fig. 1 the intensities of the (400) diffraction of the Vs = 15 m/s ribbon are about three times stronger than that of the Vs = 10 m/s and Vs = 20 m/s ribbons. It is indicated that a preferential orientation of ⟨100⟩ closely parallel to the solidification direction is obtained.

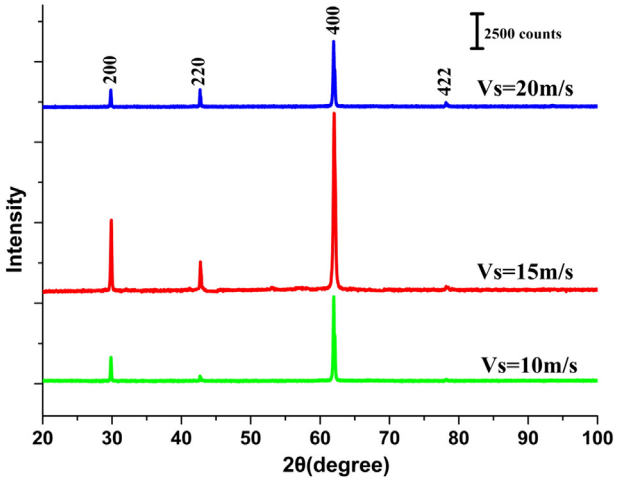

Fig. 1. X-ray diffraction (XRD) patterns of $Ni_{45}Mn_{36.6}In_{13.4}Co_5$ melt-spun ribbons prepared with different wheel speed.

3.2. Microstructure and Texture Evolution Depending on Wheel Speed

Fig. 2 is the inverse pole figure (IPF) images showing the cross section of $Ni_{45}Mn_{36.6}In_{13.4}Co_5$ ribbons. It is obvious that ordered columnar grains grow perpendicularly to the ribbon surface, but has a slight deviation. According to solidification theory the solidification process of melt spinning is affected by the transfer process of heat and momentum [35,36]. When melt alloy is ejected onto water cooled copper roll, latent heat transfers from high temperature melt alloy to the copper wheel, the heat flow direction is perpendicular to the wheel surface. At the same time, copper wheel transfers momentum to melt alloy, and the direction of momentum is paralleled to the copper surface. Under the influence of mutually perpendicular heat transmission and momentum transmission, grains grow perpendicularly to the ribbon surface with deviation of several degrees. It is noted that the deviating degree increases with velocity increasing. Amorphous ribbons can also be obtained by melt spinning, whereas if the ribbon is polycrystalline, the solidification process of melt spinning is mainly controlled by heat transfer [37]. The thickness of crystalline melt-spun ribbons (y_m) can be approximately calculated by equation as follows [35]:

$$y_m = \frac{\alpha(T_m - T_r)x_d}{r\omega(\Delta h + c\Delta T_m)} \quad (1)$$

where α is the heat transfer coefficient of wheel and melt alloy interface, T_m and T_r is the temperature of melt alloy and wheel surface respectively, ΔT_m is the superheat of melt alloy, ω is rotational angular velocity of copper wheel, r is radius of copper wheel, c is specific heat capacity of melt alloy, Δh is latent heat of solidification, x_d is length of melt alloy contact with copper wheel surface.

From Eq. (1) it can be seen that the thickness of ribbons depends mainly on $x_d/r\omega$ when a particular ribbon is fabricated. The length of melt alloy contact with copper wheel surface (x_d) increases with the rotational angular velocity of copper wheel (ω), and the x_d increasing rate is higher firstly and then lower than that of ω. So the thickness of melt-spun ribbons increases firstly and then decreases with increasing wheel speed. The thickness of ribbons prepared with wheel speed of 10 m/s, 15 m/s, 20 m/s is 42 μm, 65 μm and 30 μm, respectively, according to the IPF images in Fig. 2. The solidification of melt spinning is fast, it is